Available online at www.sciencedirect.com
ScienceDirect
Mechanics of Materials 40 (2008) 100–114
MECHANICS OF MATERIALS
www.elsevier.com/locate/mechmat

Analytical solution of anisotropic plastic deformation induced by micro-scale laser shock peening

Youneng Wang *, Jeffrey W. Kysar, Y. Lawrence Yao

Department of Mechanical Engineering, Columbia University, New York, NY 10027, United States

Received 14 September 2005; received in revised form 14 August 2006

Abstract

Laser shock peening (LSP) is a process to improve material fatigue life by introducing compressive residual surface stress in a target. The residual stresses are introduced when a high-intensity laser impinges on an ablative layer deposited on the surface of the target material. The interaction between laser and the ablative layer creates a high pressure plasma that leads to plastic deformation. If the laser spot size is of the order of a few micrometers, the potential exists to use this process to enhance the fatigue life of micro-scale components or to selectively treat highly localized regions of macroscale components. However, for such micro-scale laser shock peening (μLSP), the laser spot size is likely to be of the order of the material grain size. Therefore the material properties must be treated as anisotropic and heterogeneous rather than isotropic and homogeneous. In the present work, anisotropic slip line theory is employed to derive the stress and deformation fields caused by μLSP on single crystal aluminum which is oriented so that plane strain conditions are admitted. The predicted size of the deformed region is compared with deformation measurement by atomic force microscopy (AFM) and with lattice rotation measurement by electron backscatter diffraction (EBSD). In addition, single crystal plasticity finite element simulations are performed for the process. The results suggest that the analytical solution captures the salient features of the deformation state and is able to predict the size of the resulting plastically deformed region.

Keywords: Anisotropic; Slip line theory; Laser shock peening; Single crystal; Analytical solution

1. Introduction

Laser shock peening (LSP) is a process to improve material fatigue life by introducing compressive residual stress in the surface of the target. The residual stresses are introduced when a high-intensity laser impinges on the surface of the target material which ablates the surface and creates a high pressure plasma. The process is typically implemented with an ablative layer on the surface of the target so that the material from the target itself is not removed. It has been studied since the 1960s by a number of researchers (Clauer and Holbrook, 1981; Peyre et al., 1996; Clauer and Lahrman, 2001). Much of the previous work focused on using lasers with spot sizes of several millimeters. Recently, laser shock peening has been performed using a laser spot size of about 10 μm, with the goal

* Corresponding author. Tel.: +1 212 854 2966; fax: +1 212 854 3304.
E-mail address: eugene.wang@us.michelin.com (Y. Wang).

0167-6636/$ - see front matter © 2007 Elsevier Ltd. All rights reserved.
doi:10.1016/j.mechmat.2006.08.011

of using LSP to improve reliability and reduce failure in highly localized regions and in small components. It has been demonstrated that micro-scale laser shock peening (μLSP) has the potential to improve the reliability performance of micro-devices by efficiently inducing favorable residual stress distributions in treated surfaces (Zhang and Yao, 2000; Chen et al., 2004a,b).

An important consideration in understanding the mechanics of μLSP at the micro-scale is that the laser spot size is likely to be approximately the same as the average grain size of the target so that deformation is expected to occur predominately within a small number of grains. Thus in order to accurately model the process, the material properties must be treated as anisotropic and heterogeneous rather than isotropic and homogeneous. There is expected to be a range of possible deformation and residual stress states due to laser shock peening of an anisotropic and heterogeneous material. The ultimate goal of this research is to determine the range of possible behaviors. In order to gain insight into the deformation and stress fields associated with μLSP, it is advantageous to first apply the process to a single crystal so that the effects of the anisotropy can first be identified in a homogeneous material. Therefore, in this paper, μLSP is applied to a single aluminum crystal. Future work will concentrate on understanding the effects of heterogeneity by applying μLSP on or near the grain boundary of a bicrystal.

There are several objectives in the present work. The first is to experimentally characterize the deformation state associated with μLSP in a single crystal. The second is to employ anisotropic slip line theory to derive the stress and deformation state resulting from laser shock peening on a single crystal surface under plane strain conditions. In addition, the process of μLSP is studied from the perspective of detailed single crystal plasticity simulations using the finite element method. It should be noted that since rate and inertial effects are neglected in this study, the analytical and numerical simulations are necessarily approximate. Nevertheless, as will be seen, they do capture the general trends and thus give some insight into the laser shock peening process. Rate and inertial effects will be included in future studies.

The remainder of the paper is organized as follows. The experimental conditions and post-peening material characterization, which includes plastic deformation measurement by AFM and lattice rotation quantification by electron backscatter diffraction (EBSD) are presented in Sections 2 and 3, respectively. The principles of anisotropic slip line theory as applied to laser shock peening are reviewed in Section 4, and the derivation of stress and deformation fields under a Gaussian pressure distribution on a single crystal is presented in Section 4. In Section 5, the finite element method is used to study laser shock peening effects; the results are compared both to experimental results and also to the analytical solution by anisotropic slip line theory. Section 6 gives the concluding remarks.

2. Laser shock peening and experiment conditions

When a target is irradiated by an intense (>1 GW/cm^2) laser pulse, the surface layer vaporizes into a high temperature and pressure (1–10 GPa) plasma. The plasma induces shock waves during expansion from the irradiated surface and mechanical impulses are transferred to the target. If the plasma is confined by water or other medium, the shock pressure into the material can be magnified by a factor of 5 or more compared with the open air condition (Fox, 1974). These pressures are well above the yield stress of most metals, thus plastic deformation can be induced. As a result, if the peak shock pressure is over the Hugoniot elastic limit (HEL) of the target material for a sufficient time, compressive residual stress distribution in the surface of the irradiated volume can be induced as a consequence of the plastic deformation (Clauer and Holbrook, 1981).

In this study, a frequency tripled Q-switched Nd:YAG laser ($\lambda = 355$ nm) in TEM$_{00}$ mode was used for the μLSP experiments with a 50 ns pulse duration and a 12 μm beam diameter, as shown in Fig. 1. A thin layer of high vacuum grease (about 10 μm thick) was spread evenly on the sample surface, and a 16 μm thick polycrystalline aluminum

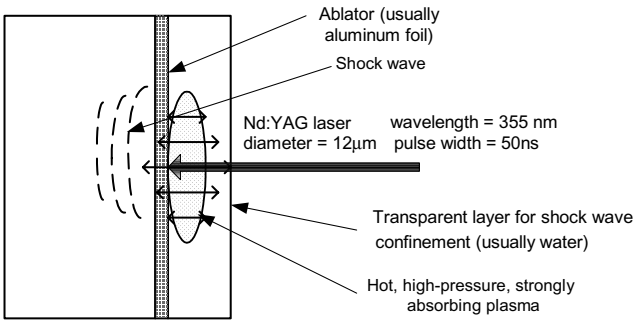

Fig. 1. Laser shock peening process.

foil, chosen for its relatively low threshold of vaporization, was tightly pressed onto the grease. The sample was placed in a shallow container filled with distilled water around 3 mm above the sample's top surface. A line of μLSP shocks was created on the sample surface with a 25 μm spacing along the [1 1 0] direction as shown in Fig. 2. A pulse energy of 228 μJ was used which corresponded to a laser intensity 4.03 GW/cm^2. After shock processing, the coating layer and the vacuum grease were manually removed. It was shown in previous work that the induced deformation is due to shock pressure and not due to thermal effects since only the ablative coating is vaporized by the laser shocking (Zhang and Yao, 2000; Chen et al., 2004a).

To investigate the response of an anisotropic material to laser shock peening, a single crystal specimen of aluminum was employed with a crystallographic orientation intended to yield a non-symmetric deformation field. The crystal was grown from the melt via the Bridgman method. It was oriented with Laue back-reflection X-ray diffraction and cut to shape with a wire electrical discharge machine (EDM) manufactured by Mitsubishi (RA-90). The newly cut surfaces were subjected to a polishing regimen which ended in a 1 μm diamond paste in oil. This was followed by electrochemical polishing to ensure that all material which was mechanically deformed during the cutting process was removed. As shown in Fig. 2, the shocked surface was $(1\,\bar{1}\,4)$ and the shocked line was parallel to the [1 1 0] direction. It was shown in previous study (Chen et al., 2004a,b) that the resulting deformation state under the shock line is approximately a two-dimensional deformation state in the (1 1 0) plane.

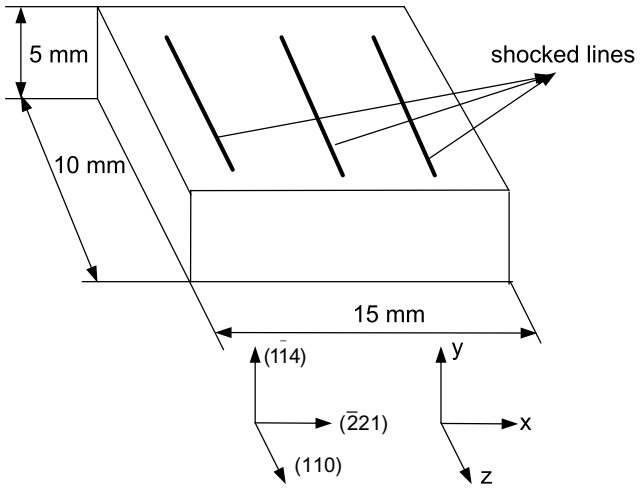

Fig. 2. Shocked line direction with respect to crystalline orientation (laser pulse energy = 228 μJ, pulse duration = 50 ns, pulse number = 3 at each location, pulse repetition rate = 1 kHz, pulse spacing = 25 μm).

3. Post-peening material characterization

3.1. Deformation measurement by atomic force microscope (AFM)

The typical deformed configuration of the shocked region was observed and measured using atomic force microscopy (Digital Instruments Nanoscope Inc.) as seen in Fig. 3a. The deformation is approximately uniform along the shocked line, which is indicative of a 2D deformation state. The detailed cross section profile, in Fig. 3b, shows that the deformation depth was about 2 μm and plastic deformation size is about 125 μm. From both three-dimensional geometry and height information in Fig. 3a, it is clear that the shocked line is surprisingly uniform deformed along [1 1 0] direction in spite of the fact that the laser shocks were created sequentially, and 25 μm apart.

3.2. Lattice orientation measurement with electron backscatter diffraction

From the work of Kysar and Briant (2002), it is possible to measure the extent as well as amount of lattice rotation induced in the crystal by the μLSP by employing electron backscatter diffraction (EBSD) to measure the crystallographic orientation as a function of position. EBSD is a diffraction technique for obtaining crystallographic orientation with sub-micron spatial resolution from bulk samples or thin layers in a scanning electron microscope.

In this study, the crystallographic orientation of the shock peened top surface was collected using EBSD, which provided information about the lattice rotation on the shocked surface. After that, in order to obtain the depth distribution and magnitude of lattice rotation below the shocked surface, the specimen was sectioned via wire electrical discharge machine (EDM) to expose a (1 1 0) plane in the center region of the specimen. The newly exposed center surface was polished and electrochemically polished as before after which the crystal orientation of the sectioned surface was mapped using EBSD.

EBSD data was collected using a system supplied by HKL Technology and attached to a JEOL JSM 5600LV scanning electron microscope. All data were acquired in the automatic mode, using external

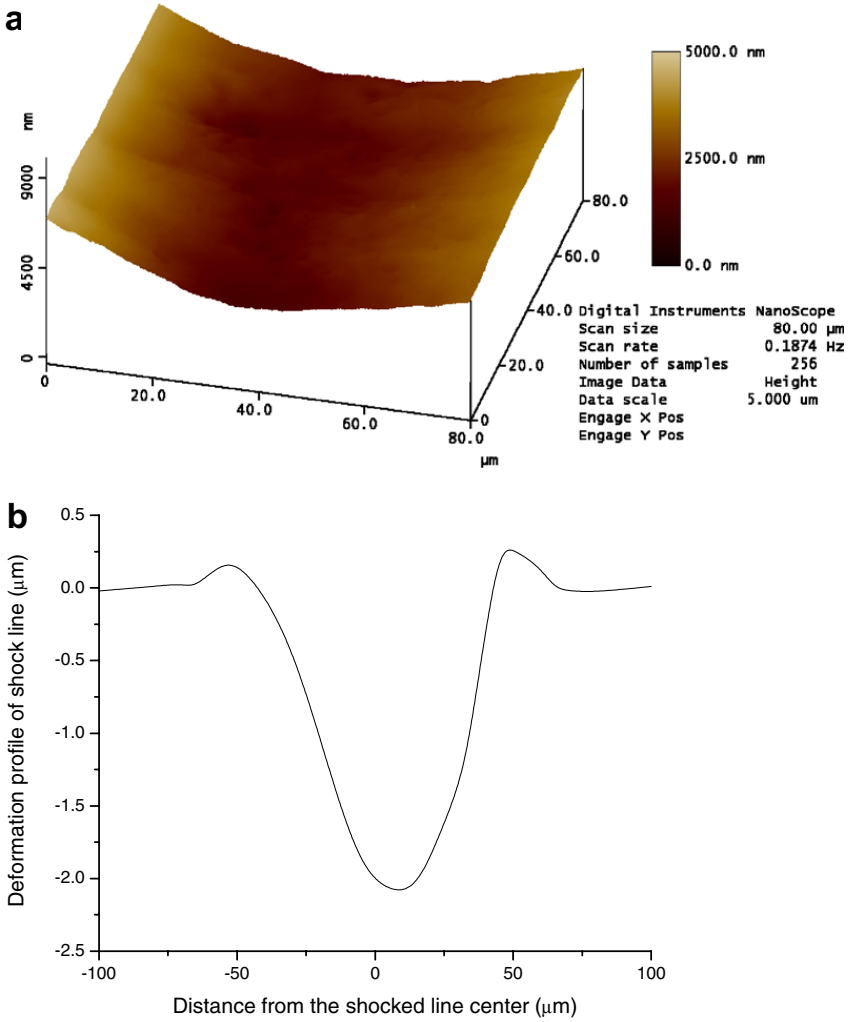

Fig. 3. Deformed geometry of shocked line for aluminum sample by using AFM: (a) three-dimensional geometry (scan area = 80 × 80 μm, data scale = 1 μm); (b) typical section geometry.

beam scanning and employing a 3 μm step size. The scan area was 320 μm × 250 μm on the shocked surface and 150 μm × 100 μm on the cross section as in Figs. 4 and 5, respectively. The EBSD results from each individual scan comprise data containing the position coordinates and the three Euler angles which describe the orientation of the particular interaction volume relative to the orientation of the specimen in the SEM, which allow the in-plane and the out-of-plane lattice rotations to be calculated relative to the known undeformed crystallographic orientation, which serves as the reference state.

3.2.1. Lattice rotation measured from the surface across the shocked line

The lattice rotation contour map on the shocked Al $(1\bar{1}4)$ sample's surface is shown in Fig. 4a. Fig. 4b shows the spatial distribution of lattice rotation along three locations across the shocked line at ordinate positions of 60 μm, 140 μm and 220 μm, respectively. The red[1] region corresponds to counter-clockwise rotation about the z-axis (as defined in Fig. 2) which is positive and the blue region corresponds to clockwise rotation which is negative. It is evident that the lattice rotation is zero (green region) far away from the shocked line which corresponds to the shock-free region. As before, the lattice rotation distribution along the shocked line is quite uniform which suggests the approximate two-dimensional deformation state mentioned before. The lattice rotation value is up to ±2° between ±55 μm from the center of shocked line

[1] For interpretation to color in Fig. 4, the reader is referred to the web version of this article.

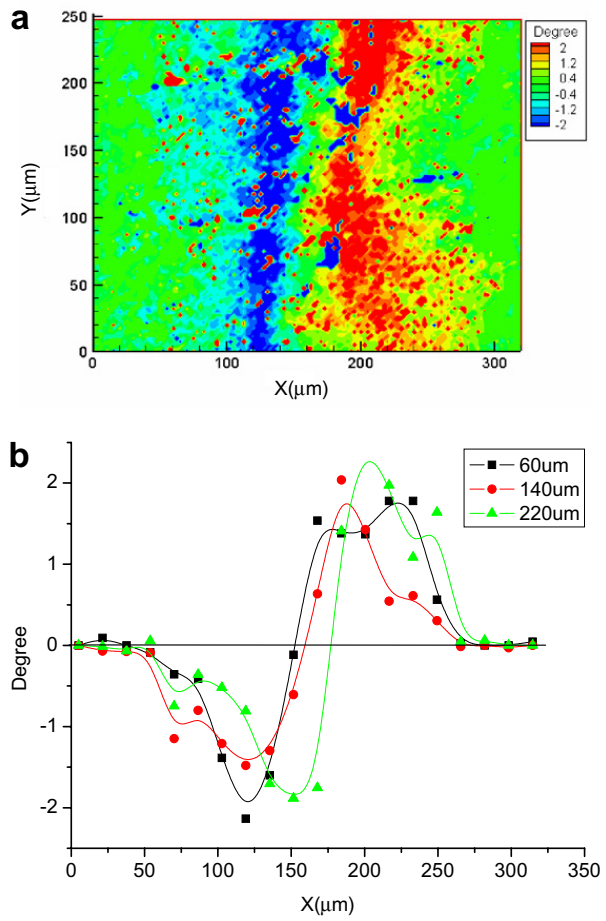

Fig. 4. (a) Lattice rotation contour map on sample surface; (b) lattice rotation distribution along three cross section lines corresponding to y-position of 60 μm, 140 μm and 220 μm of Fig. 8a, respectively. Positive rotation is counter-clockwise about the z-axis.

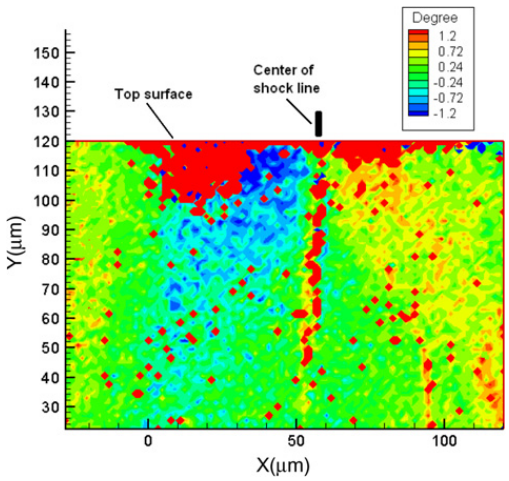

Fig. 5. Lattice rotation contour map on the (1 1 0) cross section. Positive rotation is counter-clockwise about the z-axis.

and the rotation direction is anti-symmetric on both sides of shocked line.

3.2.2. Lattice rotation measured from cross section perpendicular to shocked line

From the measurement mentioned above, we obtained the lattice rotation result on the laser shock peened surface. In order to measure the lattice rotation below the sample surface and study the spatial distribution in the depth direction, the sample was sectioned on a (1 1 0) plane via wire EDM and the crystallographic orientation of the newly exposed surface was mapped using EBSD. The lattice rotation obtained in this manner is called "in-plane" because the experimental results indicate an approximate two-dimensional deformation state.

Fig. 5 shows the lattice rotation in the cross section. The lattice rotation varies between ±1.2° in the region up to 60 μm below the sample surface, however it was not possible to measure the lattice rotation directly at the free surface because the edge was rounded slightly during polishing. In the center of the shock line, the lattice rotation is nearly zero (green[2]) and rotation direction reversed across the shocked line, which is consistent with the result from sample surface. The maximum lattice rotation occurs near the sample surface and the value decays as depth increases.

4. Anisotropic slip line theory solution for laser shock peening

In this section, we present results of elementary analytical predictions of the stress and deformation fields associated with laser shock peening in anisotropic, homogeneous materials. Since the surface deformation and lattice rotation under laser shock peening indicate that an approximate two-dimensional deformation state exists, we assume that the induced deformation state is strictly two-dimensional, which may be a gross oversimplification. However, it turns out that such an approach can shed significant insight into the mechanics of deformation which will be useful to predict the overall plastic deformation size. LSP poses many significant challenges, because of the high transient pressures, fluid–solid interaction and high strain rates in single crystal media at the micrometer length scale. Given the absence of constitutive data in this strain rates and pressures of interest, it is impossible to incorporate realistically these effects into the analytical

[2] For interpretation to color in Fig. 5, the reader is referred to the web version of this article.

analysis. The goal of the analytical analysis is then to attempt to understand the overall character of the deformation and stress fields and see how much can be predicted by such a simple anisotropic slip line theory.

4.1. Anisotropic slip line theory

Slip line theory for isotropic rigid-plastic materials was developed by Hencky (1923) and Prandtl (1923) and extended by Hill (1950) to include anisotropy for rigid-ideally plastic materials with ellipsoidal yield surfaces. Booker and Davis (1972) and Rice (1973) generalized the theory for a general anisotropic rigid-ideally plastic material with arbitrary anisotropic convex yield contours. Based on the general theory, the stress field associated with a two-dimensional punch indenting an anisotropic rigid-ideally plastic material was derived. In particular, Rice (1973) derived the solution appropriate for punch indentation of a single crystal. Also, Rice (1987) derived the solution associated with crack tip fields in single crystals using similar concepts. Both solutions exhibit the common feature of center-fan constant stress regions which are centered at the edge of the punch and the crack tip, respectively. The solution for the punch in a single crystal assumed that the pressure distribution under the punch was uniform.

There are two significant differences between Rice's (1973) derivation of the fields under an indenter in an anisotropic plastic material and that of the present work. The first is that it is typical to assume a constant pressure distribution beneath an indenter as it penetrates a surface, whereas it is known (Zhang and Yao, 2000) that the pressure due to ablation of the ablative layer associated with LSP can often be approximated as having a Gaussian distribution. Second, the geometry of an indenter is well-defined so that a singular point exists at the edge of the indenter which serves at the transition point from a constant stress state to the centered fan. In the case of LSP, it is not evident how to precisely determine the position of a singular point, or for that matter, whether the singular points exist.

The derivation presented herein for the stress and deformation state associated with LSP accounts for both these differences. To address the non-uniform pressure distribution, we use an analytical technique from Kysar et al. (2005) which allows a heterogeneous stress state to be derived in a region of single slip based upon traction boundary conditions in single crystals. To address the question of the position of the singular points, we employ a scaling argument to derive an approximate position relative to the center of the Gaussian pressure distribution. It is expected that this position is accurate to within a constant factor of the order of magnitude of unity. Detailed numerical simulations are then used to determine the value of the constant.

Solutions obtained with slip line theory are approximate in the sense that only the equilibrium equations and the rigid ideally plastic constitutive equations are satisfied, whereas the compatibility and strain–displacement relations are ignored. In addition, the deformation field is required to be one of plane strain. The resulting governing partial differential equation is hyperbolic and the associated characteristics are termed α- and β-lines. Specifically for single crystal plasticity under conditions of single slip, the α-lines correspond to the direction of slip and the β-lines correspond to slip plane normal in regard of single slip, so that the characteristics in such regions form an orthogonal net.

4.1.1. Plane strain condition

For a face-centered cubic crystal of aluminum, there are a total of twelve plastic slip systems $\{1\,1\,1\}\langle 1\,1\,0\rangle$ within a crystal. If a line loading is applied parallel to a $\langle 1\,1\,0\rangle$ direction in a FCC crystal, certain slip systems act cooperatively which enable plane deformation conditions to be achieved (Rice, 1987). As discussed in detail by Kysar and Briant (2002) and Kysar et al. (2005), the $(1\,\bar{1}\,1)[0\,1\,1]$ and $(1\,\bar{1}\,1)[\bar{1}\,0\,1]$ slip systems can act cooperatively and in equal amounts to form an effective in-plane slip system which induces plastic deformation in the $[\bar{1}\,1\,2]$ direction which lies within the $(1\,1\,0)$ plane. This effective in-plane slip system is denoted as slip system (i) in Fig. 6. Likewise, the $(\bar{1}\,1\,1)[1\,0\,1]$ and $(\bar{1}\,1\,1)[0\,\bar{1}\,1]$ slip systems can act cooperatively and in equal amounts to form an effective slip system which induces plastic deformation in the $[1\,\bar{1}\,2]$ direction which lies within the $(1\,1\,0)$ plane. This effective in plane slip system is denoted as slip system (iii) in Fig. 6. Similarly, the $(1\,1\,1)[\bar{1}\,1\,0]$ and $(1\,1\,\bar{1})[\bar{1}\,1\,0]$ slip systems act cooperatively and in equal amounts to form an effective slip system which induces plastic deformation in the $[\bar{1}\,1\,0]$ direction which lies within the $(1\,1\,0)$ plane. This effective in plane slip system is denoted as slip system (ii) in Fig. 6. Thus, a loading which can be approximated as a distributed line loading

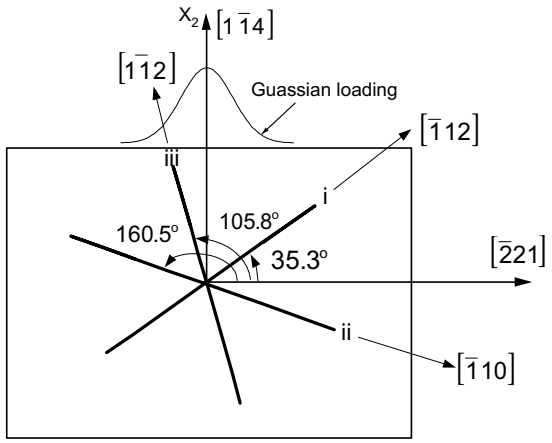

Fig. 6. Plane strain slip systems corresponding to $(1\,\bar{1}\,4)$ orientation.

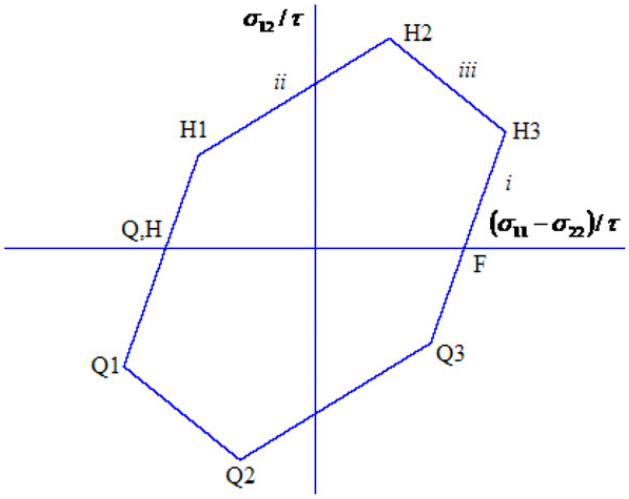

Fig. 7. Yield surface contour for $(1\,\bar{1}\,4)$ orientation.

along $[1\,1\,0]$ generates a predominately plane deformation state in $(1\,1\,0)$ plane. Rice (1987) showed that the remaining slip systems do not contribute significantly to sustained in-plane plastic deformation.

The yield contour which corresponds to the above plane strain conditions can be determined based upon Schmid's law (e.g. Hertzberg, 1995). For a plane deformation state, Schmid's law can be succinctly expressed as (e.g. Kysar et al., 2005)

$$\sigma_{12} = \tan 2\phi_j \left(\frac{\sigma_{11}-\sigma_{22}}{2}\right) \pm \frac{\beta_j \tau_j}{\cos 2\phi_j} \tag{1}$$

where ϕ_j is the angle of the jth slip system relative to the abscissa of the global spatial coordinate system, τ_j is the critical resolved shear stress on the jth slip system, and β_j is a geometrical constant, $\beta_1 = \beta_3 = 2/\sqrt{3}$ and $\beta_2 = \sqrt{3}$ as discussed in Rice (1987). Eq. (1) represents a pair of parallel lines in the stress space for which $(\sigma_{11}-\sigma_{22})/2$ is the abscissa and σ_{12} is the ordinate. Clearly the slope of the lines in stress space relative to the $(\sigma_{11}-\sigma_{22})/2$ axis is $2\phi_j$ as shown in Fig. 7. Since there are three effective slip systems, there are six lines in stress space. The inner envelope of these lines forms the yield contour, which has the property that plastic slip can occur whenever the stress state is such that it lies on the yield contour in stress space. Further, the active slip system is determined by the side of the yield contour on which the stress state lies. The positions of the vertices in stress space are listed in Table 1.

For the particular case considered in this paper, a semi-infinite homogenous rigid ideally plastic single crystal is studied under plane strain conditions. As shown in Fig. 6, the distributed pressure loading is applied to the $(1\,\bar{1}\,4)$ surface and the plane of deformation is $(1\,1\,0)$. Quasi-static loading instead of shock loading is assumed in order to first study only the effect of anisotropy. In addition, the critical resolved shear stress τ is assumed to be the same for each slip system. Compared with the actual process conditions of laser shock peening, the assumptions employed in the analytical solution based are grossly oversimplified, however this approach helps to determine the aspects of the stress and deformation state which are a consequence of the anisotropy of plastic deformation.

Table 1
Yield surface vertices

Vertex	$(\sigma_{11}-\sigma_{22})/2\tau$	σ_{12}/τ
H_1	$-\frac{7}{18}\sqrt{6}$	$\frac{4}{9}\sqrt{3}$
H_2	$\frac{1}{4}\sqrt{6}$	$\sqrt{3}$
H_3	$\frac{23}{36}\sqrt{6}$	$\frac{5}{9}\sqrt{3}$
F	$\frac{1}{2}\sqrt{6}$	0
Q_3	$\frac{7}{18}\sqrt{6}$	$-\frac{4}{9}\sqrt{3}$
Q_2	$-\frac{1}{4}\sqrt{6}$	$-\sqrt{3}$
Q_1	$-\frac{23}{36}\sqrt{6}$	$-\frac{5}{9}\sqrt{3}$
Q	$-\frac{1}{2}\sqrt{6}$	0

The shape of the yield contour determines the details of the deformation and stress state. As seen in Fig. 7, the yield condition for slip system (i) intersects the $(\sigma_{11}-\sigma_{22})/2\tau$ axis at points F and Q, H.[3] From the Gaussian pressure distribution boundary conditions, it is evident that on the entire shocked

[3] The points Q and H are coincident in stress space. Nevertheless, this terminology is adopted to simplify later descriptions of the derived stress state.

surface so that the stress state on the shocked surface will be either at F or at the point denoted Q, H in Fig. 7. Since σ_{22} is significantly less than zero underneath the center of the pressure distribution, it is expected that the stress state will be at point F. Far away from the center of the pressure distribution σ_{22} will approach zero and it is expected that σ_{11} will be negative, so that the equilibrated stress state will be at point Q, H. Therefore conditions of single slip on the same slip system are expected to occur under the center region of the pressure distribution as well as far away from the center, and that centered fan structures will join the two regions.

4.1.2. Geometry of slip line field near the center of the Gaussian pressure distribution

The stress state under the Gaussian pressure distribution can be derived by constructing the network of α- and β-lines according the procedures in Kysar et al. (2005). The α-line can be identified as corresponding to slip direction and the β-line can be identified as corresponding to the slip plane normal of the active slip system in single slip regions.

The Gaussian pressure loading can be thought of as a "punch", with a non-uniform pressure distribution. However, it is not obvious what the effective width of the punch is. In order to estimate the effective width we will first find the uniform pressure below which we do not expect to activate plastic deformation. In order to do that we temporarily assume that a uniform pressure of magnitude P^* is applied to the $(1\,\bar{1}\,4)$ surface and we seek the value of P^* at which plastic deformation initiates. We then approximate the half-width of the punch as that distance away from the center of the Gaussian pressure distribution at which the applied pressure is equal to P^*. This allows us to determine the scaling relationship for the punch width to within a dimensionless constant, and we subsequently rely on numerical simulations to precisely determine the value of the constant.

Considering a uniaxial uniform pressure loading P^*, the boundary conditions on the free surface are $\sigma_{12}=0$, $\sigma_{11}=0$ and $\sigma_{22}=-P^*$. Therefore, $(\sigma_{11}-\sigma_{22})/2$ is greater than zero and $\sigma_{12}=0$, which corresponds to point F in Fig. 7; that is, only slip system (i) will be activated directly underneath the loading when the plastic slip occurs. Thus, the applied stress state can be resolved onto a local coordinate system, for which the x_1'-axis is parallel to the $[\bar{1}\,1\,2]$ direction and the x_2'-axis is parallel to $[1\,\bar{1}\,1]$. The resolved shear stress on slip system (i) can thus be obtained as:

$$\sigma_{12}' = \frac{\sigma_{22}}{2}\sin 2\phi_1 = \frac{-P^*}{2}\sin 2\phi_1 \tag{2}$$

where ϕ_1 is the angle between the orientations of $[\bar{2}\,2\,1]$ and $[\bar{1}\,1\,2]$, which is 35.3°. Equating σ_{12}' with the effective critical resolved shear stress, $A=\beta_1\tau$, one can solve for the value of P^* at which plastic deformation initiates

$$P^* = \mp\frac{2A}{\sin 2\phi_1}. \tag{3}$$

For the Gaussian pressure distribution

$$P(x) = P_0\exp\left(-\frac{x^2}{2R^2}\right) \tag{4}$$

where R is the radius of plasma, it is easily seen that this pressure P^* is attained at approximate "punch" radius x_p' as follows

$$x_p' = \sqrt{2}R\sqrt{\ln\left(\frac{P_0}{2A}\right)+\ln(\sin 2\phi_1)}. \tag{5}$$

For the plane strain condition with the Gaussian loading, the actual "punch" radius should scale with Eq. (5), i.e.

$$x_p = cx_p' \tag{6}$$

where c is a dimensionless constant of order unity which will be determined from detailed numerical simulation.

4.1.3. Stress underneath the punch

From the applied pressure loading boundary in Eq. (4) and the assumption that plastic deformation occurs according to Eq. (1), the full stress state on the shocked surface for $|x_1|\leqslant x_p$ and $x_2=0$

$$\sigma_{11}(x,0) = -P_0\exp\left(-\frac{x^2}{2R^2}\right)+\frac{2A}{\sin 2\phi_1} \tag{7}$$

$$\sigma_{22}(x,0) = -P_0\exp\left(-\frac{x^2}{2R^2}\right) \tag{8}$$

$$\sigma_{12}(x,0) = 0 \tag{9}$$

With the assumption of a homogenous rigid ideally plastic material, for which plastic deformation is occurring on a single slip system everywhere within a certain region, it is evident that the resolved shear stress σ_{12}' is constant within that region. Since only one slip system is active, the characteristic α-lines are parallel to the active slip system and the β-lines are parallel to the slip plane normal. It then follows

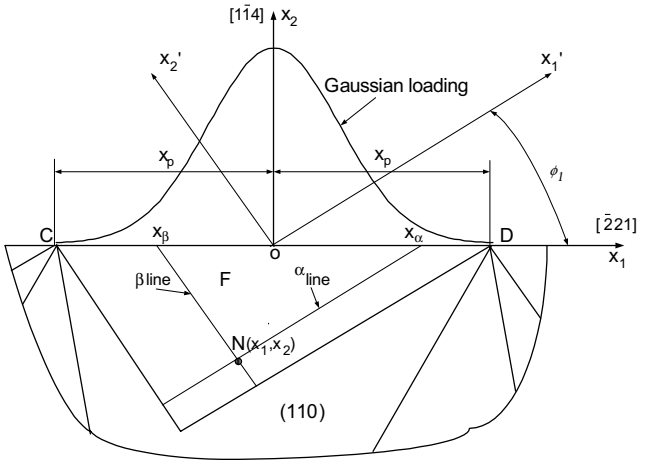

Fig. 8. Plastic deformation zone F directly underneath a Gaussian loading.

directly from equilibrium (e.g. Kysar et al., 2005) that σ'_{11} is a constant on each α-line and σ'_{22} is a constant on each β-line, where the primed stresses are calculated with respect to the local coordinate system in Fig. 8. For traction boundary conditions, the value of σ'_{11} and σ'_{22}, respectively, for each α- and β-line can be determined by the values of σ'_{11} and σ'_{22} on the boundary. Therefore, we resolve the stress state on the surface into the components in the local coordinate system to obtain on the free surface:

$$\sigma'_{11} = -P_0 \exp\left(-\frac{x^2}{2R^2}\right) + \frac{A}{\sin 2\phi_1}(1+\cos 2\phi_1) \tag{10}$$

$$\sigma'_{22} = -P_0 \exp\left(-\frac{x^2}{2R^2}\right) + \frac{A}{\sin 2\phi_1}(1-\cos 2\phi_1) \tag{11}$$

$$\sigma'_{12} = \beta_1 \tau \tag{12}$$

Since σ'_{11} along an α-line and σ'_{22} along β-line are constant, the stresses at each point beneath the punch in the local primed coordinate system can be obtained from the surface stresses as shown in Eqs. (10) and (11). From Fig. 8, it can be shown that the α-line and β-line associated with a point N in the region beneath the center of the punch intersect the free surface at x_α and x_β, respectively at

$$x_\alpha = x_1 - x_2 \cot\phi_1 \tag{13}$$

and

$$x_\beta = x_1 + x_2 \tan\phi_1 \tag{14}$$

Therefore, the stresses σ'_{11} and σ'_{22} at point $N(x_1, x_2)$ are equal to the stresses on the surface $\sigma'_{11}(x_\alpha)$ and $\sigma'_{22}(x_\beta)$, respectively. From Eqs. (10)–(14), there results

$$\sigma'_{11}(x_1,x_2) = -P_0 \exp\left(-\frac{(x_1 - x_2\cot\phi_1)^2}{2R^2}\right) + \frac{A}{\sin 2\phi_1}(1+\cos 2\phi_1) \tag{15}$$

$$\sigma'_{22}(x_1,x_2) = -P_0 \exp\left(-\frac{(x_1 + x_2\tan\phi_1)^2}{2R^2}\right) \frac{A}{\sin 2\phi_1}(1-\cos 2\phi_1) \tag{16}$$

$$\sigma'_{12}(x_1,x_2) = -A \tag{17}$$

The overall region within which these expressions are valid consists of the locus of all points N for which the associated α- and β-lines intersect the surface in the region $|x_1| \leqslant x_p$ for $x_2 = 0$ as shown in Fig. 8. This region forms a triangle with vertices at $(x_p, 0)$, $(-x_p, 0)$ and $\left(\frac{x_\alpha \tan^2\phi_1 + x_\beta}{1+\tan^2\phi_1}, \frac{(x_\beta - x_\alpha)\tan\phi_1}{1+\tan^2\phi_1}\right)$.

4.1.4. Geometry of other regions and their stresses

Beyond the radius of the "punch", the loading $P(x_1)$ is assumed have a negligible effect on the plastic deformation so it is set to zero to give operative boundary conditions of $\sigma_{12}(x_1, 0) = 0$ and $\sigma_{22}(x_1, 0) = 0$ for $|x_1| > x_p$. Since σ_{11} is compressive for $|x_1| > x_p$ the yield point for these regions corresponds to the coincident points H and Q in Fig. 7 when plastic slip occurs. We expect single slip regions denoted as H and Q to exist near the free surface beyond the punch as indicated in Fig. 9.

Since the stress state on the surface of region F is at point F on the yield surface and in the adjacent regions on the surface the stress state is at points

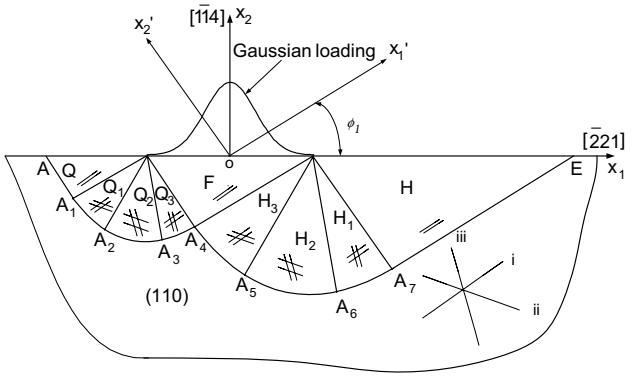

Fig. 9. Geometry of anisotropic slip line field under a Gaussian loading.

H and Q, there must exist a transition zone so that the stress state beneath the punch at point F on the yield surface can transition to the stress state H and Q outside of the punch. Rice (1973) explained why a centered fan region is expected to exist at both edges of a punch. The stresses when expressed in Cartesian coordinates are constant within each angular sector of the centered fan. These fields follow from the assumptions that the stresses do not vary in the radial direction and also that the material is at yield at all points. The boundaries between the angular sectors represent discontinuities of stress. Further, the discontinuities correspond only to slip directions and slip plane normals acting through the center of the fan. The stress within each angular sector corresponds to a vertex on the yield surface, so that in general, two slip systems are active. Therefore, the boundaries between angular sectors correspond to sides of the yield surface.

As seen in Fig. 7, the trajectory of the stress must begin at point F and has to follow the yield contour to reach the stress state H or Q because plastic deformation is assumed to occur. Upon applying the concepts of Rice (1987), the centered fan structure at both edges of the Gaussian punch is shown in Fig. 9, where the regions marked by H_1, H_2, H_3, Q_1, Q_2, and Q_3 within the centered fans corresponds to the vertices H_1, H_2, H_3, Q_1, Q_2, and Q_3 respectively on the yield contour of Fig. 7. From F to Q, the stress trajectory is along the bottom portion of the yield contour because σ_{12} is expected to be negative in this region due to the presence of pressurized region to its right. Similarly, from F to H, the stress state is along the top portion of the yield contour.

For the regions H and Q, the boundary conditions are $\sigma_{12}=0$, $\sigma_{22}=0$ on the surface, so from Eq. (1) we find that $\sigma_{11}=-2A/\sin 2\phi_1$. The stresses in zones Q_i and H_i, where $i=1, 2, 3$, are determined following the method developed by of Rice (1973, 1987) where the relationship between change of $\sigma=\frac{1}{2}(\sigma_{11}+\sigma_{22})$, denoted $\Delta\sigma$, and the change of the arc length ΔL, around the yield surface is given as

$$\frac{1}{2}\Delta(\sigma_{11}+\sigma_{22})=-\Delta L \tag{18}$$

The arc length L around the yield surface has units of stress and increases as $Q\to Q_1\to Q_2\to Q_3\to F$ and $H\to H_1\to H_2\to H_3\to F$. The change of the arc length L can be calculated if the yield surface vertices are known, which is determined by the geometry of the yield contour of Fig. 7 as listed in Table 1. Thus, by using Eq. (18) and the yield contour of Fig. 7, the stress states in each constant region of the centered fan can be found as listed in Table 2 (e.g. Kysar and Briant, 2002).

Table 2
Stresses within sectors

Sector	σ_{11}/τ_{cr}	σ_{22}/τ_{cr}	σ_{12}/τ_{cr}	Active slip systems
H	$-\sqrt{6}$	0	0	(i)
H_1	$-\frac{11}{9}\sqrt{6}$	$-\frac{4}{9}\sqrt{6}$	$\frac{4}{9}\sqrt{3}$	(i) & (iii)
H_2	$-\frac{4}{3}\sqrt{6}$	$-\frac{11}{6}\sqrt{6}$	$\sqrt{3}$	(ii) & (iii)
H_3	$-\frac{13}{9}\sqrt{6}$	$-\frac{49}{18}\sqrt{6}$	$\frac{5}{9}\sqrt{3}$	(i) & (ii)
Q_3	$-\frac{16}{9}\sqrt{6}$	$-\frac{23}{9}\sqrt{6}$	$-\frac{4}{9}\sqrt{3}$	(i) & (iii)
Q_2	$-\frac{5}{3}\sqrt{6}$	$-\frac{7}{6}\sqrt{6}$	$-\sqrt{3}$	(ii) & (iii)
Q_1	$-\frac{14}{9}\sqrt{6}$	$-\frac{5}{18}\sqrt{6}$	$-\frac{5}{9}\sqrt{3}$	(i) & (ii)
Q	$-\sqrt{6}$	0	0	(i)

As shown in Fig. 9, we expect a region of single slip below the punch and two regions of single slip to exist beyond the punch. Also, there must be two centered fans to transition stress states between the single slip regions. Based on the geometry of this slip line field, we can estimate the size of plastically deformed region, from point A to E, as

$$\begin{aligned} L &= 2x_p(1+\cot\phi_1+\tan\phi_1)\\ &= 2\sqrt{2}cR(1+\cot\phi_1+\tan\phi_1)\\ &\quad\times\sqrt{\ln\left(\frac{P_0}{2A}\right)+\ln(\sin 2\phi_1)} \end{aligned} \tag{19}$$

5. Finite element simulation

In the analytical solution by anisotropic slip line theory, we make several simplifying assumptions, such as loading cut-off, rigid ideally plastic deformation, plane strain conditions, etc. This allowed the dominant features of plasticity associated with μLSP anisotropic plastic materials to be determined, while neglecting rate effects. One of most interesting features of the solution is the presence of discontinuities associated with the central fan regions. The effects of these assumptions on the overall deformation field can be systematically investigated by individually relaxing them in the context of numerical simulations. In this section, the effect of relaxing the assumption of a sharp cut-off in the applied pressure is presented. One item of interest is to investigate the predicted discontinuities in more

detail. Their existence is predicated on the assumption of a sharp cut-off and it is of interest to see if they manifest themselves under a Gaussian loading which has no explicit cut-off radius. The numerical simulation also will allow a more precise definition of the cut-off radius. In addition, the lattice rotation is calculated numerically and residual stress can be estimated. Subsequent simulations which account for more realistic material constitutive behavior, as well as accounting for inertial contributions, will concentrate on how the additional effects modify the baseline solution. Thus, it is expected that these simulations will lay the ground work for more realistic simulations.

5.1. FEM simulation conditions

Finite element simulations based on the theory of single crystal plasticity (Asaro, 1983) were carried out with a user-material subroutine (UMAT), which was written by Huang (1991) and modified by Kysar (1997). It is incorporated into the finite element analysis using the general purpose finite element program ABAQUS/Standard. In the UMAT, the $\{1\,1\,1\}\langle 1\,1\,0\rangle$ slip systems in FCC metal are employed and a critical resolved shear strength $\tau_{\mathrm{CRSS}} \approx 1$ MPa is assumed for each of the slip systems, which is a reasonable value for high purity single crystals employed (e.g. Kysar, 2001). The element used in the simulation was a plane strain reduced integration, hybrid element (CPE4RH) and total simulation size is 384 μm × 192 μm (thickness × width). The mesh size is about 0.1 μm in the area close to the loading and 1.5 μm far away from the loading. As for boundary conditions of the plane strain model, the applied surface tractions correspond to the applied pressure on the shocked surface. At the bottom surface, the vertical displacement is specified to be zero and the outer edges are traction free. In the simulation, elastic-ideally plastic behavior is assumed so that hardening is neglected, in order to compare the results to the approximate analytical solution. The simulation ignores rate and inertial effects. These idealizations will be relaxed in future studies.

The pressure distribution on the surface is Gaussian as that in Eq. (4), where x is the radial distance from the center of the laser beam and R is the radius of plasma. The radius of the laser beam used in the experiments is 6 μm with a 50 ns pulse duration. Following Zhang and Yao (2001) the resulting plasma radius is $R = 9.5$ μm at the end of the laser pulse. The plasma is expected to expand further after 50 ns, but the resulting pressure decreases very quickly (Zhang and Yao, 2000, 2001) so that effect is ignored. The peak value of pressure is assumed to be $P_0/\tau_{\mathrm{CRSS}} = 7$. In the simulation, the magnitude of the pressure is increased linearly from zero with time until it reaches its maximum at 15 ns, after which it remains constant until the end of 50 ns. The loading is applied in this manner so that the fields are not propagating quasistatically at the end of the simulation. In the finite element analysis, the stresses, strains and lattice rotation were solved incrementally by ABAQUS using a finite strain kinematic structure described by Huang (1991). A power-law rate-dependent relationship proposed by Hutchinson (1968), and described by Connolly and McHugh (1999), Huang (1991), Kysar (2001), Peirce et al. (1983), and Savage et al. (2004) was used:

$$\dot{\gamma}_k = \dot{\gamma}_0 \operatorname{sgn}(\tau_k) \left\{ \left| \frac{\tau_k}{g_k} \right| \right\}^m \tag{20}$$

where is $\dot{\gamma}_0$ the reference strain rate, τ_k is the applied resolved shear stress, m is the rate sensitivity exponent, and g_k is related to critical resolved shear stress of the kth-slip system, as given by Peirce et al. (1983). In this simulation, $\dot{\gamma}_0 = 10^{-3}$ and $m = 50$, which yields a nearly rate-independent constitutive response.

5.2. Finite element simulation results

5.2.1. Punch radius and plastic deformation size

The punch radius can be determined by comparing the plastic deformation in the FEM simulation to the geometry of anisotropic slip line field predicted analytically as shown in Fig. 9. The plastic deformation in the simulation is characterized by the increment of total slip during an increment of loading once the maximum pressure has been applied, as shown in Fig. 10d. The slip increment, rather than the accumulated slip, is employed in order to compare the deformation in the fully established deformation state to the approximate analytical solution. By scaling the geometry of the anisotropic slip line field to the pattern of total shear strain, the punch radius can be determined as about 20.3 μm. Therefore, the constant in Eq. (6) can be evaluated from Eq. (5) as $c = x_{\mathrm{p}}/x'_{\mathrm{p}} = 20.3/9.3 = 2.18$. In order to explore the validity of this result, a simulation was performed for which the shocked surface was $[1\,\bar{1}\,6]$ and the x_1-axis coincides with $[\bar{3}\,3\,1]$ so that $\phi_1 = 41.5°$. The resulting punch radius

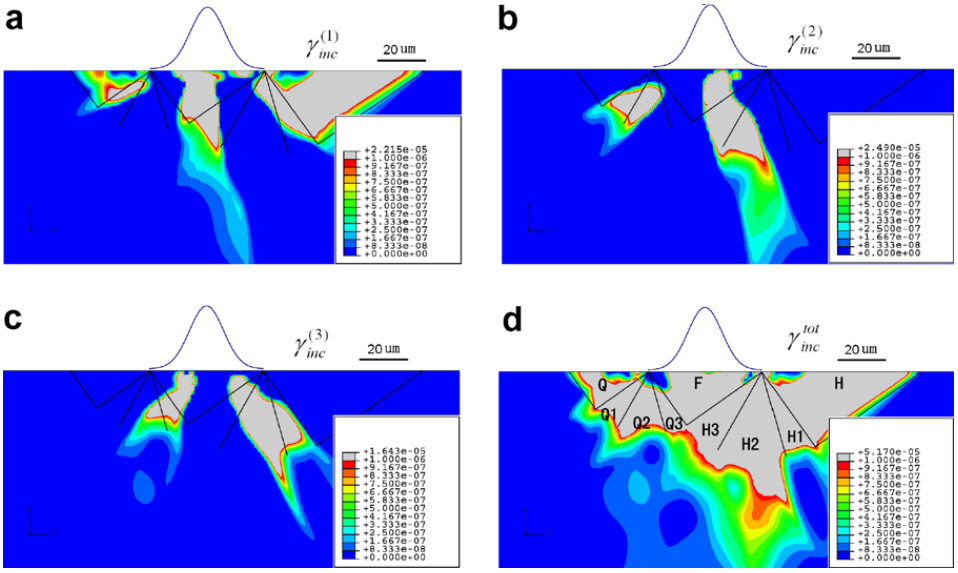

Fig. 10. Shear strain increment in each slip system in the end of loading step: (a) increment in slip system (i); (b) increment in slip system (ii); (c) increment in slip system (iii); (d) total shear strain increment.

was 13.1 μm so that $c = 20.6/9.46 = 2.18$. Hence, the region over which plastic deformation occurs can be estimated using Eq. (19) as

$$L = 2x_p(1 + \cot\phi_1 + \tan\phi_1) = 127\ \mu\text{m} \tag{21}$$

which is close to that measured by AFM of approximately 125 μm, however it is somewhat smaller than the width of the region of significant plastic deformation as measured by EBSD in Fig. 4a. This discrepancy might be resolved by accounting for the rate and inertial effects, as well as more accurately modeling the pressure distribution of the plasma.

As discussed in the derivation of the analytical solution, various slip system are expected to be activated within certain regions of the deformation field according to Fig. 9 and Table 2. Hence, it is of interest to investigate the slip which occurs on individual slip system in the simulation. Therefore the shear strain increment for each slip system is plotted in Fig. 10a–c. It can be seen that only slip system (i) is active in region H and Q, as predicted by the analytical solution. In region F, mainly slip system (i) is active, but with small contribution of slip systems (iii) and (ii) away from the center of the loading. In the center-fan regions, the slip system activated in each fan is in accordance with the analytical solution; that is, slip system (iii) is mainly active in fans H_1, H_2, Q_2 and Q_3 as shown in Fig. 10a and slip system (ii) is mainly active in fans H_2, H_3, Q_1 and Q_2 as shown in Fig. 10b. Also, slip system (i) is active in fans H_1, H_3, Q_1 and Q_3.

5.2.2. Stress distribution

From the analytical solution, for region F we expect σ'_{11} to be constant along α-lines in the slip direction of (i) and σ'_{22} to be constant along the corresponding β-lines. Results from the simulation for σ'_{11} and σ'_{22} are shown in Fig. 11. It can be seen from Fig. 11b and c that the analytical predictions are reflected in the center region of region F. However, near the edges (or at the punch radius) the analytical predictions do not hold. This can be explained by the fact that there exists a region under each edge of the putative punch with a positive σ_{11} as shown in Fig. 11a, which is not predicted by the analytical solution. These regions of $\sigma_{11} > 0$ cause the punch edge to be diffuse, rather than sharp.

In addition, the stress $\sigma = (\sigma_{11} + \sigma_{22})/2$ should be constant in regions H and Q since it is equal to $-A/\sin 2\phi_1$. The plot of σ as shown in Fig. 11d indicates two constant regions corresponding to regions H and Q. Also, there are narrow regions, over which the stress state changes rapidly. It can be seen that at least three of the regions of rapid stress variation correspond to the boundaries between H and H_1, H_1 and H_2, and Q and Q_1.

The predicted distribution of σ_{11} residual stress after unloading is shown in Fig. 12. The compressive residual stress close to the surface is balanced by the tensile stress far from the surface and most of area close to the surface has a compressive residual stress except for two small regions of tensile residual stress. The results of compressive σ_{11} are

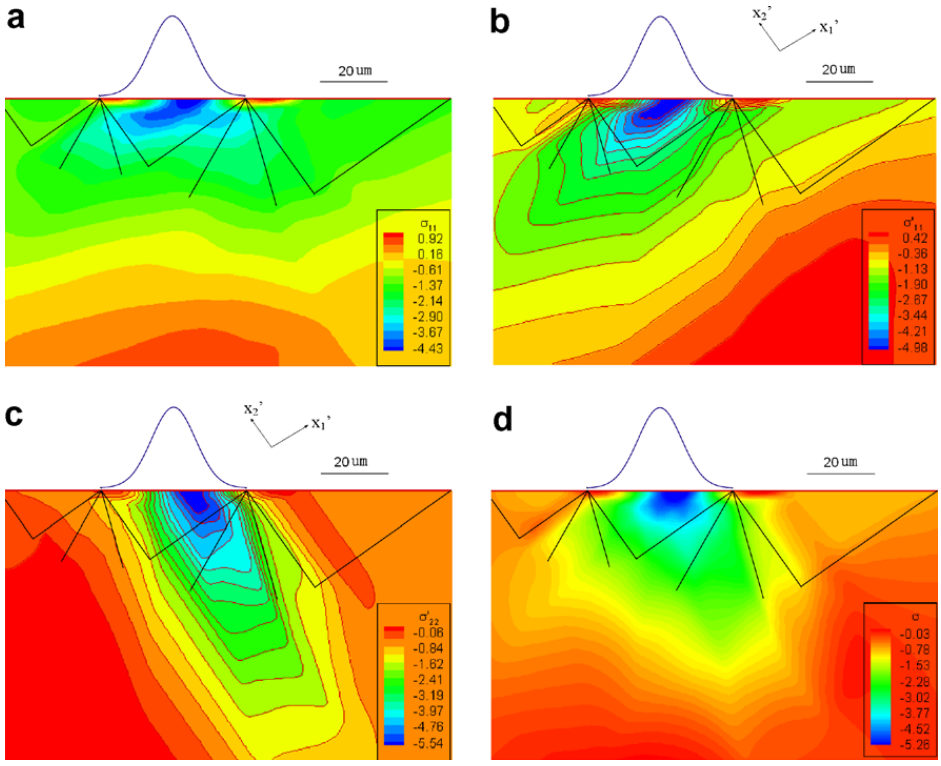

Fig. 11. Stress distributions in the end of loading: (a) σ_{11} in the original coordinate system; (b) σ'_{11} in the primed coordinate system; (c) σ'_{22} in the primed coordinate system; (d) $\sigma = (\sigma_{11} + \sigma_{22})$.

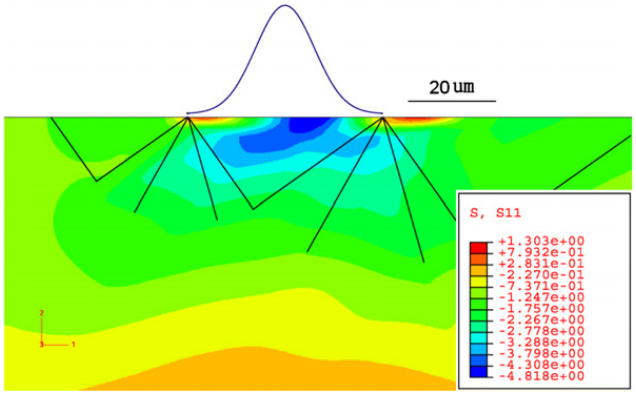

Fig. 12. FEM simulation of residual stress distribution.

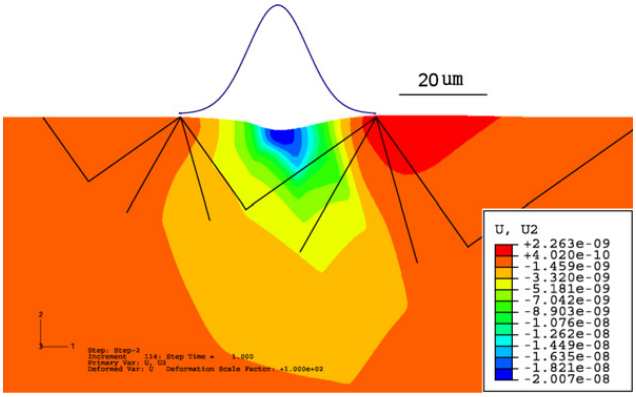

Fig. 13. FEM simulation of normal displacement distribution with the deformation scale factor 100.

beneficial to the fatigue life improvement after μLSP processing. Also, normal displacement contour shown in Fig. 13 indicates the same trend as measured by AFM, i.e. deformed downward in the center while deformation on two sides of the punch is upward.

5.2.3. Lattice rotation result and comparison with that of EBSD

As discussed in Chen et al. (2004b), crystal lattice rotation occurs during laser shock peening due to plastic deformation. Fig. 4 illustrates an EBSD measurement of the lattice rotation which occurs during μLSP for the shocked region on the sample's top surface. In this contour, the green regions (angle = 0°) on the two sides correspond to the shock free region since there is no change from the original crystal orientation. The blue and red scales indicate a deviation of the $[1\,\bar{1}\,4]$ crystal axis from the sample surface normal; the maximum angle is approximately two degrees. The lattice rotation close to center of shocked region is close to zero and increases with distance from the center before

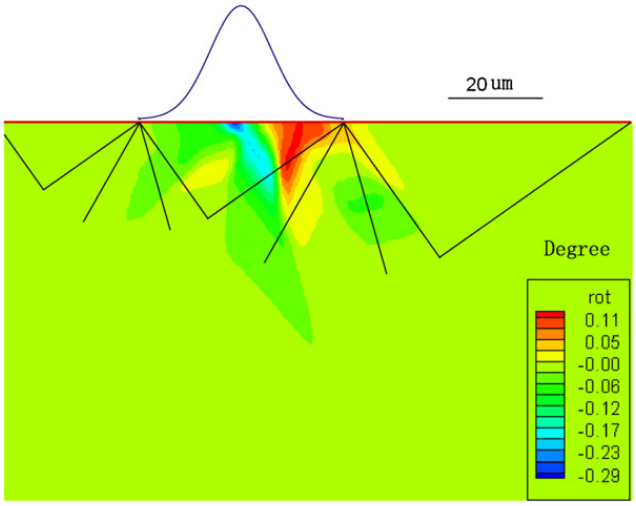

Fig. 14. Lattice rotation contour by FEM.

decreasing. The maximum rotation occurs about 35 μm away from the center and the overall region with significant orientation change is about 200 μm. The lattice rotation from FEM simulation shown in Fig. 14 indicates two distinct misorientation regions on each side which is similar to the EBSD results. Also, it is clear that there is a misorientation free region in the middle which can be seen from the experimental results of Figs. 4a and 5, as well. It is expected that inclusion of hardening, rate and inertial effects will be necessary in order to obtain a better correlation of the simulations with experiment.

6. Conclusions

In this paper, the plastic deformation induced by μLSP on a single crystal aluminum with orientation $[1\bar{1}4]$ was investigated using anisotropic slip line theory. It was found that single slip conditions prevail in certain regions and that the potential exists for rapid changes in field variables. Also, stresses were derived in each region of slip line field. There are two constant stress regions beyond the punch radius denoted as Q and H and two center-fans. An elementary FEM simulation was carried out to find the putative "punch" radius as well as to study the effects of relaxing the assumptions used in the analytical solution, however future simulations need to account for rate and inertial effects as well as more accurately model the time and spatial evolution of the plasma pressure distribution. The plastic deformation size by anisotropic slip line theory and simulation is predicted to be approximately 127 μm, which is in reasonable agreement with 125 μm of AFM measurement, but is smaller than that measured by EBSD. Regions of rapid change of field variables are predicted by FEM which correspond to those by predicted analytically. EBSD measurements indicate that up to 2° lattice rotation was induced by μLSP with the given laser energy 228 μJ and the FEM simulation shows a similar trend of the lattice rotation distribution. The analytical methodology presented herein enhances the understanding of anisotropic behavior of μLSP peening process and is now possible to apply this theory to analyze the plastic deformation size and the distribution trend of residual stresses. Thus, the application of anisotropic slip line theory can shed some insight to understand the process of plastic deformation induced by μLSP.

Acknowledgement

This work is supported by the National Science Foundation under grant DMI-02-00334. JWK would like acknowledge support by the National Science Foundation under the Faculty Early Career Development (CAREER) Program with grant CMS-0134226. This work has used the shared experimental facilities that are supported primarily by the MRSEC Program of the National Science Foundation under Award Number DMR-0213574 and by the New York State Office of Science, Technology and Academic Research (NYSTAR).

References

Asaro, R.J., 1983. Micromechanics of crystals and polycrystals. Adv. Appl. Mech. 23, 1–115.

Booker, J.R., Davis, E.H., 1972. A general treatment of plastic anisotropy under conditions of plane strain. J. Mech. Phys. Solids 20, 239–250.

Chen, H., Yao, Y.L., Kysar, J.W., 2004a. Spatially resolved characterization of residual stress induced by micro scale laser shock peening. J. Manuf. Sci. Eng. 126, 226–236.

Chen, H., Kysar, J.W., Yao, Y.L., 2004b. Characterization of plastic deformation induced by micro scale laser shock peening. J. Appl. Mech. 71, 713–723.

Clauer, A.H., Holbrook, J.H., 1981. Effects of laser induced shock waves on metals. Shock Waves and High Strain Phenomena in Metals – Concepts and Applications. Plenum Press, New York, pp. 675–702.

Clauer, A.H., Lahrman, D.F., 2001. Laser shock processing as a surface enhancement process. Key Eng. Mater. 197, 121–142.

Connolly, P., McHugh, P., 1999. Fracture modelling of WC–Co hard metals using crystal plasticity theory and the Gurson model. Fatigue Fract. Eng. Mater. Struct. 22, 77–86.

Fox, J.A., 1974. Effect of water and paint coatings on laser-irradiated targets. Appl. Phys. Lett. 24, 461–464.

Hencky, H., 1923. Über einige statisch bestimmte Fälle des Gleichgewichts in plastischen Körpern". Z. Angew. Math. Mech. 3, 241–251, in German).

Hertzberg, R.W., 1995. Deformation and Fracture Mechanics of Engineering Materials, fourth ed. John Wiley and Sons, New York.

Hill, R., 1950. The Mathematical Theory of Plasticity. Clarendon Press, Oxford.

Huang, Y., 1991. A user-material subroutine incorporating single crystal plasticity in the ABAQUS finite element program, Mech Report 178, Division of Applied Sciences, Harvard University, Cambridge, MA.

Hutchinson, J.W., 1968. Singular behavior at the end of a tensile crack tip in a hardening material. J. Mech. Phys. Solids 16, 13–31.

Kysar, J.W., 1997. Addendum to "A user-material subroutine incorporating single crystal plasticity in the ABAQUS finite element program, Mech Report 178", Division of Engineering and Applied Sciences, Harvard University, Cambridge, MA.

Kysar, J.W., 2001. Continuum simulations of directional dependence of crack growth along a copper/sapphire bicrystal interface: Part I, experiments and crystal plasticity background. J. Mech. Phys. Solids 49, 1099–1128.

Kysar, J.W., Briant, C.L., 2002. Crack tip deformation fields in ductile single crystals. Acta Mater. 50, 2367–2380.

Kysar, J.W., Gan, Y.X., Mendez-Arzuza, G., 2005. Cylindrical void in a rigid-ideally plastic single crystal I: anisotropic slip line theory solution for face-centered cubic crystals. Int. J. Plast. 21, 1461–1657.

Peirce, D., Asaro, R., Needleman, A., 1983. Material rate dependence and localised deformation in crystalline solids. Acta Metall. Mater. 31, 1951–1976.

Peyre, P., Fabbro, R., Merrien, P., Lieurade, H.P., 1996. Laser shock processing of aluminium alloys, application to high cycle fatigue behaviour. Mater. Sci. Eng. A: Struct. Mater.: Properties Microstruct. Process. A210, 102–113.

Prandtl, L., 1923. Anwendungsbeispiele zu einem henckyschen salt über das plastische gleichgewicht. Zeitschr. Angew. Math. Mech. 3, 401–406.

Rice, J.R., 1973. Plane strain slip line theory for anisotropic rigid/plastic materials. J. Mech. Phys. Solids 21, 63–74.

Rice, J.R., 1987. Tensile crack tip fields in elastic-ideally plastic crystals. Mech. Mater. 6, 317–335.

Savage, P., Donnell, B.P.O., McHugh, P.E., Murphy, B., Quinn, D., 2004. Coronary stent strut size dependent stress–strain response investigated using micromechanical finite element models. Ann. Biomed. Eng. 32, 202–211.

Zhang, W., Yao, Y.L., 2000. Micro scale laser shock processing of metallic components. ASME J. Manuf. Sci. Eng. 124, 369–378.

Zhang, W., Yao, Y.L., 2001. Micro-scale laser shock processing: modeling, testing, and microstructure characterization. ASME J. Manuf. Process. 3, 128–143.